Journal of Materials Chemistry C

Impact of molecular structure on singlet and triplet exciton diffusion in phenanthroline derivatives

Journal:	*Journal of Materials Chemistry C*
Manuscript ID	TC-ART-02-2020-000716.R1
Article Type:	Paper
Date Submitted by the Author:	13-Mar-2020
Complete List of Authors:	Rai, Deepesh; University of Minnesota Twin Cities, Chemical Engineering and Materials Science Bangsund, John; University of Minnesota Twin Cities, Chemical Engineering and Materials Science García-Barriocanal, Javier; University of Minnesota College of Science and Engineering, Characterizaterization Facility Holmes, Russell; University of Minnesota Twin Cities, Chemical Engineering and Materials Science

SCHOLARONE™
Manuscripts

Impact of molecular structure on singlet and triplet exciton diffusion in phenanthroline derivatives

Deepesh Rai[1], John S. Bangsund[1], Javier Garcia Barriocanal[2] and Russell J. Holmes[1]

[1]Department of Chemical Engineering and Materials Science, University of Minnesota,

[2]Characterization Facility, University of Minnesota, Minneapolis, MN 55455

ABSTRACT

We demonstrate the impact of subtle changes in molecular structure on the singlet and triplet

exciton diffusion lengths (L_D) for derivatives of the archetypical electron-transport material

4,7-diphenyl-1,10-phenanthroline (BPhen). Specifically, this work offers a systematic

characterization of singlet and triplet exciton transport in identically prepared thin films,

highlighting the differing dependence on molecular photophysics and intermolecular spacing.

For luminescent singlet excitons, photoluminescence quenching measurements yield an L_D

from <1 nm for BPhen, increasing to (5.4 ± 1.2) nm for 2,9-dichloro-4,7-diphenyl-1,10-

phenanthroline (BPhen-Cl$_2$) and (3.9 ± 1.1) nm for 2,9-dimethyl-4,7-diphenyl-1,10-

phenanthroline (BCP). The diffusion of dark triplet excitons is probed using a phosphorescent

sensitizer-based method where triplets are selectively injected into the material of interest, with

those migrating through the material detected via energy transfer to an adjacent,

phosphorescent sensitizer. Interestingly, the triplet exciton L_D decreases from (15.4 ± 0.4) nm

for BPhen to (8.0 ± 0.7) nm for BPhen-Cl$_2$ and (4.0 ± 0.5) nm for BCP. The stark difference in

behavior observed for singlets and triplets with functionalization is explicitly understood using

long-range Förster and short-range Dexter energy transfer mechanisms, respectively.

1

INTRODUCTION

Excitons play a central role in the design of optoelectronic devices based on organic semiconductors, with exciton spin strongly determining the luminescence and transport characteristics of the component active materials.[1–5] In terms of exciton transport, spin singlet and triplet excitons diffuse via different mechanisms, due mainly to the fact that singlets may undergo radiative recombination while triplets are often dark.[6] This difference in mechanism also implies that the handles available for tuning the exciton diffusion length (L_D) may enhance the transport of one spin state while not favorably impacting the other.[7] Reduced intermolecular spacing is typically considered as a route to improve exciton transport however, even here care must be taken to avoid increasing non-radiative decay and reducing the exciton lifetime. Several studies have reported on the role of molecular functionalization and crystallization in enhancing singlet exciton transport.[8–16] There are however fewer studies of triplet excitons as they are often non-radiative and hence incompatible with common photoluminescence-based techniques. Furthermore, few efforts have sought to systematically compare the role of functionalization on both singlet and triplet states.[17,18] As such, there exists a need for experimental methodologies that permit the investigation of singlet and triplet diffusion in a common set of samples that could experimentally elucidate the fundamental difference in transport behavior between these states.

Exciton diffusion is frequently described as an ensemble of intermolecular energy transfer events with the diffusivity (D) written in terms of the energy transfer rate (k_{ET}) as: [6,10,19]

$$D = \frac{1}{6} \Sigma_N \, d^2 k_{ET}(d) = \frac{L_D^2}{\tau} \qquad (1)$$

where d is the intermolecular spacing assuming a cubic lattice, τ is the exciton lifetime and N

is the number of molecular hopping sites. For fluorescent singlet excitons, energy transfer via

dipole coupling (Förster transfer) often dominates, with a transfer rate given as:[6,20]

$$k_F(d) = \frac{1}{\tau}\left(\frac{R_0}{d}\right)^6 \qquad (2)$$

where τ is the exciton lifetime and R_0 is the Förster radius which is separately defined as:[6,12]

$$R_0^6 = \frac{9\eta_{PL}\kappa^2}{128\pi^5}\int\frac{\lambda^4 F_D(\lambda)\sigma_A(\lambda)d\lambda}{n(\lambda)^4} \qquad (3)$$

where η_{PL} is the photoluminescence efficiency, κ is the dipole orientation factor (taken as

$0.845\sqrt{\frac{2}{3}}$ for randomly oriented rigid dipoles),[21] n is the wavelength dependent refractive index

of the donor film, F_D is the normalized fluorescence spectrum, σ_A is the acceptor absorption

cross-section, and λ is the wavelength. It is clear in Eqs. 2 and 3 that a change in intermolecular

spacing can have a nuanced effect on Förster transfer. For example, prior work has shown that

an increase in L_D can be observed with increased spacing due to favorable increases in the

exciton lifetime and self-Förster radius with spacing.[12,22,23]

In materials with non-luminescent triplet excitons, energy transfer is typically mediated by

electron exchange interactions in the form of Dexter transfer. The subsequent transfer rate is

defined as:[6,19,24]

$$k_T = \frac{2\pi}{\hbar}K^2\exp\left(-\frac{2d}{L}\right)\int F_D(E)\sigma_A(E)dE \qquad (4)$$

Where F_D and σ_A are normalized donor and acceptor emission and absorption spectra,

respectively, d is the intermolecular separation, L is the effective average orbital radius for the

excited and unexcited state of donor and acceptor, and K is a constant that reflects the specific

orbital interactions. Clearly, increased intermolecular spacing hinders the triplet hopping rate

via electron exchange, making possible different trends in the dependence of L_D on spacing for singlets and triplets.

In this work, we examine singlet and triplet exciton diffusion as a function of molecular functionalization in phenanthroline derivatives, offering a useful contrast of the factors governing the migration of each state. Phenanthrolines have long been used as electron transport materials and exciton blocking layers in organic light-emitting devices (OLEDs) and organic photovoltaic cells (OPVs), and are examined here for the availability of several derivatives namely, 4,7-diphenyl-1,10-phenanthroline (BPhen), 2,9-dichloro-4,7-diphenyl-1,10-phenanthroline (BPhen-Cl$_2$), and 2,9-dimethyl-4,7-diphenyl-1,10-phenanthroline (BCP), where steric bulk and intermolecular spacing are tailored by substitution of -H, -Cl and -CH$_3$ on the phenanthroline core (Fig. 1a). Changes in intermolecular spacing also lead to changes in molecular photophysics, and measurements of exciton transport are complemented by detailed spectroscopic investigations. Thus, a systematic understanding for the role of functionalization on singlet and triplet diffusion is established.

2. EXPERIMENTAL SECTION

BPhen, BPhen-Cl$_2$, BCP, mCP and HATCN are purchased from Luminescence Technology Corporation; PtOEP is purchased from Frontier Scientific. For thickness dependent PL quenching measurements, a unity quenching efficiency is assumed for HATCN due to favorable energy offset for electron transfer.[23,25] Photoluminescence spectra are measured in a Photon Technology International QuantaMaster 400 Fluorometer equipped with a photomultiplier detection system. Structures are excited using a Xe lamp attached to a

monochromator, at an angle of 70° from substrate normal. Photoluminescence efficiencies are measured in an integrating sphere using a previously published methodology.[26] The thin film thicknesses and material optical constants are measured using a J. A. Woollam variable-angle spectroscopic ellipsometer. Singlet exciton lifetimes are measured using a PicoQuant time correlated single photon counting (TCSPC) system, pumped using a regeneratively amplified Ti:sapphire laser system producing ~80 fs, $\lambda = 900$ nm pulses at a repetition rate of 40 MHz. A $\lambda = 300$ nm excitation pulse is then obtained using a nonlinear harmonic generation system equipped with a BBO crystal for tripling the frequency of the excited pulse. A closed cycle Janis CSS-150 He optical cryostat is used to measure triplet photoluminescence spectra and lifetimes at 10 K. Samples are pumped at a wavelength of $\lambda = 337$ nm using a N_2 laser which provides ~ 1 ns pulse width. The emission spectrum from the sample is detected using a FERGIE integrated spectrograph (Princeton Instruments), with spectrum acquisition triggered externally with a pulse generator after a 5 ms delay from the laser pulse. The repetition rate of the laser is kept at 0.25 Hz. Triplet photoluminescence spectra are measured for different delay times to obtain the triplet lifetime. X-ray reflectivity is measured on a 20-nm-thick film of the active material deposited on a Si substrate using a PANalytical X'pert Pro instrument. The experimental data is simulated using GenX software to obtain thin film density, surface roughness and film thickness. The film thickness is independently checked with values from ellipsometer. The film crystallinity is checked using X-ray diffraction measurements at an incident angle of 8 degrees, while sample is being scanned using a 2D detector which spans from $2\theta = 1$ degree to 53 degrees. Experimental data for singlet and triplet L_D measurements

5

is fitted using a non-linear least square methodology where error in the fit value represents 95% confidence interval.

3. RESULTS AND DISCUSSION

Figure 1b shows the thin film extinction coefficient and photoluminescence (PL) behavior of the active materials of interest in this work. The PL collected at room temperature is fluorescence from the singlet state. The phosphorescence spectra shown in Fig. 1b were collected at 10 K at long times under pulsed laser excitation. Spectrum acquisition was triggered by a pulse generator with a 5 ms delay after the laser pulse to reject short time luminescence and only collect long-lived triplet phosphorescence. As-deposited films showed no evidence of crystallinity in X-ray diffraction (XRD) measurements. Fine differences in the intermolecular spacing with functionalization were probed by measuring film density using X-ray reflectivity (XRR). The film thickness, density, and roughness are used as fitting parameters for XRR experimental data analysis. The fit parameters along with independent measurements of film thickness using ellipsometry are shown in Table S1. XRR analysis yields extracted molecular densities of (1.87 ± 0.03) nm^{-3} for BCP, (2.04 ± 0.03) nm^{-3} for BPhen-Cl$_2$, and (2.26 ± 0.03) nm^{-3} for BPhen, consistent with previous reports for BPhen and BCP.[27]

The singlet L_D for each material of interest is extracted using thickness dependent PL quenching.[28,29] Thin film fluorescence is measured with and without the presence of an adjacent top quenching layer of 1,4,5,8,9,11-hexaazatriphenylene hexacarbonitrile (HATCN).[28] The PL ratio (quenched to unquenched) is measured as a function of active layer thickness and fit to yield the singlet L_D. Table 1 lists the singlet L_D values extracted for BPhen and its derivatives,

6

obtained by analytical modelling of the associated PL ratio (Fig. 2). Extracted values of L_D are

< 1 nm for BPhen, (3.9 ± 1.1) nm for BCP, (5.4 ± 1.2) nm for BPhen-Cl$_2$. It is worth noting

that if fit explicitly, the data in Fig. 2 for BPhen yields $L_D = (0.8 \pm 0.3)$ nm. This value is

below the estimated resolution limit of 1 nm of the technique.

The observed trend in singlet L_D can be considered in terms of Förster theory by

considering how changes in intermolecular spacing and the self-R_0 (Table 1) impact L_D. Singlet

L_D values for the BPhen derivatives scale linearly with the ratio R_0^3/d^2 as expected based on

Eqs. 1 and 2. This ratio is largest for BPhenCl$_2$, which reflects a high degree of spectral overlap

between fluorescence and absorption spectra.

Figure 3a shows the device architecture for measuring the triplet L_D in BPhen and its

derivatives using a phosphorescent sensitizer based method.[30,31] A layer of (4,6-

difluorophenyl)pyridinato-C2,N](picolinato)iridium(III) (FIrpic) (triplet energy, $E_T = 2.65$ eV)

injects triplets into the phenanthroline of interest ($E_T = 2.47$ eV for all three materials). Injected

triplets that migrate through the full thickness of the active layer are detected using a sensitizer

of platinum octaethylporphyrin (PtOEP) ($E_T = 1.9$ eV)[32] doped in the wide energy gap host 1,3-

bis(N-carbazolyl)benzene (mCP) ($E_T = 2.9$ eV). Exciton diffusion in the active layer is defined

in terms of a transport efficiency (η_T) as:[31-32]

$$\eta_T = \frac{\Delta PL^{PtOEP}}{\Delta PL^{FIrpic}} \times \frac{\eta_{FIrpic}^{PL}}{\eta_{PtOEP}^{PL}} \quad (5)$$

Where η_{FIrpic}^{PL} and η_{PtOEP}^{PL} are the outcoupled PL efficiencies of the FIrpic and PtOEP layers.

The outcoupling efficiency ratio in the absence of the active layer is experimentally determined

by directly injecting excitons from FIrpic to PtOEP using a previously published method.[30,31]

The variation in outcoupling efficiency as a function of active layer thickness is calculated using Setfos 4.6 (Fluxim) software (Fig. S2).

Figure 3b shows PL spectra for FIrpic and PtOEP with an active layer of BPhen, BPhen-Cl_2, or BCP, for cases with and without injection of excitons into the active layer. The increase in PL from PtOEP due to energy transfer from FIrpic can be isolated from direct optical excitation (*i.e.* where the injection layer of FIrpic is replaced with mCP). Kinetic Monte Carlo (KMC)[30,31] modelling of the experimentally measured η_T as a function of active layer thickness results in triplet L_D values of (15.4 ± 0.4) nm for BPhen, (8.0± 0.7) nm for BPhen-Cl_2, and (4.0 ± 0.5) nm for BCP (Fig. 4a).

The mechanism for energy transfer can be understood by first decoupling the exciton lifetime and the diffusivity. The triplet lifetime for each material is shown in Table 1 and was determined from low temperature transient phosphorescence. The trend in triplet lifetime (Table 1, Fig. S3) cannot alone explain the observed variation in triplet L_D, suggesting a change in diffusivity. This could come from changes in optical overlap, the molecular orbital radius, and the intermolecular spacing. Changes in film roughness could also lead to differences in the extracted L_D, but this possibility is ruled out using atomic force microscopy (AFM) of as-deposited films of each active material. Films of all materials studied here show a featureless morphology with root mean square roughness < 1 nm (Fig. S4).

The variation in triplet diffusivity is considered in terms of differences in intermolecular spacing. Indeed, Eqs. 1 and 4 suggest an exponential relationship between triplet diffusivity and intermolecular spacing, and hence the linearity of a semi-log plot between triplet (L_D/d)

and intermolecular spacing can be used to check the validity of the assumed diffusion model.

Figure 4b shows a linear fit between a semi-log plot of L_D/d and intermolecular spacing. The

value of d is determined by taking the cube root of the molecular density ($\sqrt[3]{\frac{1}{\rho}}$) as measured

using XRR. The intermolecular spacing varies in increasing order as (7.62 ± 0.04) Å for BPhen,

(7.88 ± 0.04) Å for BPhen-Cl$_2$ and (8.11 ± 0.04) Å for BCP, corresponding-well with the

concomitant reduction in triplet L_D. The observed linear trend also holds for a mixture of 10

wt.% BCP in BPhen, suggesting that BCP and BPhen form a substitutional solid solution. The

slope of the plot yields the molecular orbital radius as $(0.37 \pm 0.04$ Å) (Fig. 4b). This value is

consistent with previous reports for Dexter transfer yielding ~ 0.39 Å to 2.1 Å.[33–37]

4. CONCLUSIONS

We present a study connecting the measured singlet and triplet exciton diffusion length with

changes in molecular structure and intermolecular spacing. The singlet L_D values are extracted

using thickness dependent photoluminescence quenching measurements while the triplet L_D

values are extracted using a phosphorescent sensitizer-based methodology. For the

phenanthroline derivatives considered here, the intermolecular spacing varies in increasing

order as (7.62 ± 0.04) Å for BPhen, (7.88 ± 0.04) Å for BPhen-Cl$_2$, and (8.11 ± 0.04) Å for

BCP. The singlet L_D increases from $L_D <1$ nm for BPhen to (5.4 ± 1.2) nm for BPhen-Cl$_2$, and

(3.9 ± 1.1) nm BCP, while the triplet L_D decreases from (15.4 ± 0.4) nm for BPhen to $(8.0 \pm$

0.7) nm for BPhen-Cl$_2$, and (4.0 ± 0.5) nm for BCP. The variation in singlet L_D is understood

using Förster transfer, considering changes in the intermolecular spacing as well as factors like

the photoluminescence efficiency and optical overlap.   The decrease in triplet L_D is understood

more simply using Dexter transfer where the rate of energy transfer scales exponentially with intermolecular spacing.   This work offers insight into the significant and differing role changes in molecular structure can play for singlet and triplet exciton transport.

ASSOCIATED CONTENT

Supporting Information: Simulated and experimental X-ray reflectivity (XRR) data used to obtain thin film density. Simulated outcoupled photoluminescence efficiency ratio as a function of active layer thickness for calculation of transport efficiency. Triplet exciton lifetimes extracted from transient photoluminescence. Thin film surface morphology extracted using AFM.

Conflicts of Interest

There are no conflicts of interest to declare.

ACKNOWLEDGMENTS

Table 1: Exciton transport and photophysical parameters for phenanthroline thin films

| Materials	Singlet L_D (nm)	Singlet τ (ns)	Singlet η_{PL} (%)	Self-R_0 (nm)	Triplet L_D (nm)	Triplet τ (ms) (10 K)
BPhen	<1	0.58 ± 0.03	2.5 ± 0.5	0.59 ± 0.01	15.4 ± 0.4	455.2 ± 7.9
BPhen-Cl$_2$	5.4 ± 1.2	0.48 ± 0.01	9.4 ± 0.9	0.84 ± 0.01	8.0 ± 0.7	313.7 ± 19.5
BCP	3.9 ± 1.1	1.24 ± 0.01	21.6 ± 2.2	0.85 ± 0.01	4.0 ± 0.5	633.1 ± 59.8
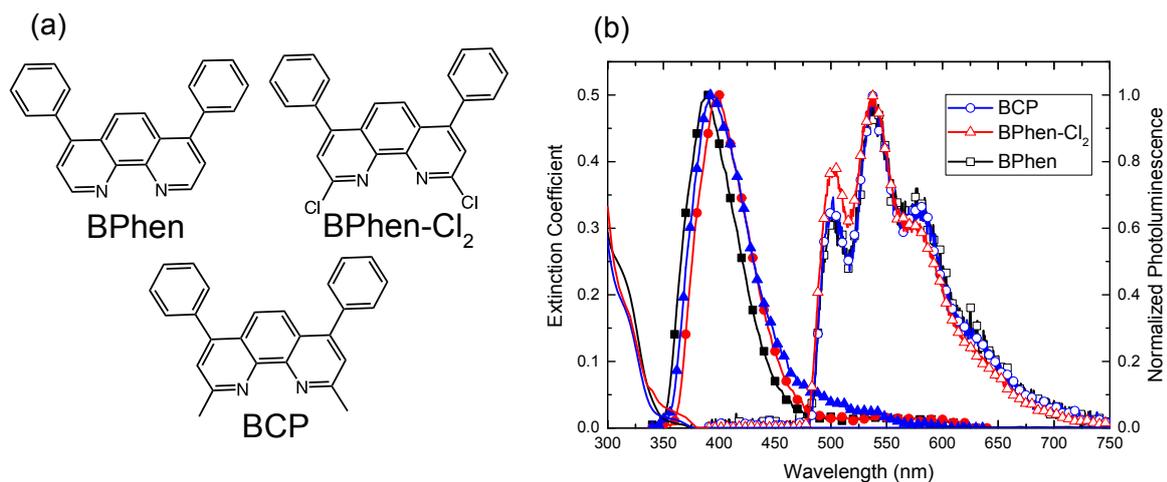
Figure 1: (a) Molecular structures of the phenanthroline derivatives considered in this work.(b)

Thin film fluorescence (closed symbols) and extinction spectra (solid lines) for the molecules

in (a) taken at room temperature. Low temperature phosphorescence spectra (open symbols)

are collected at 10 K at long-times after pulsed excitation to avoid detection of fluorescence.
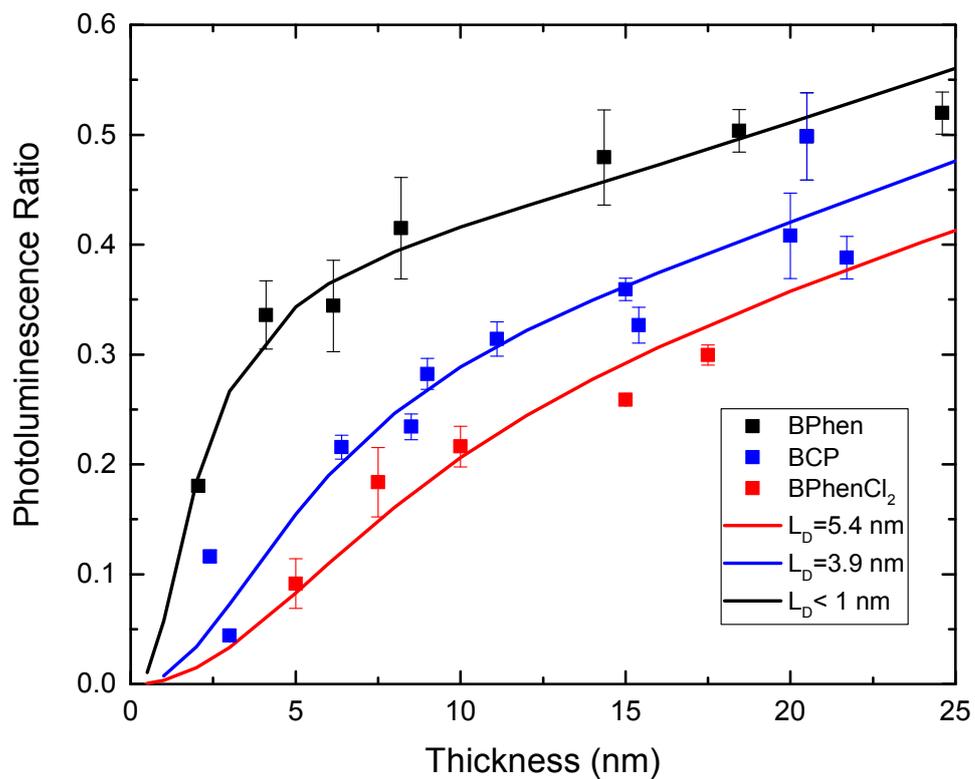
Figure 2: Photoluminescence ratios (with and without an adjacent HATCN quenching layer) for BPhen and its derivatives with the corresponding exciton diffusion length (L_D) extracted from the data.
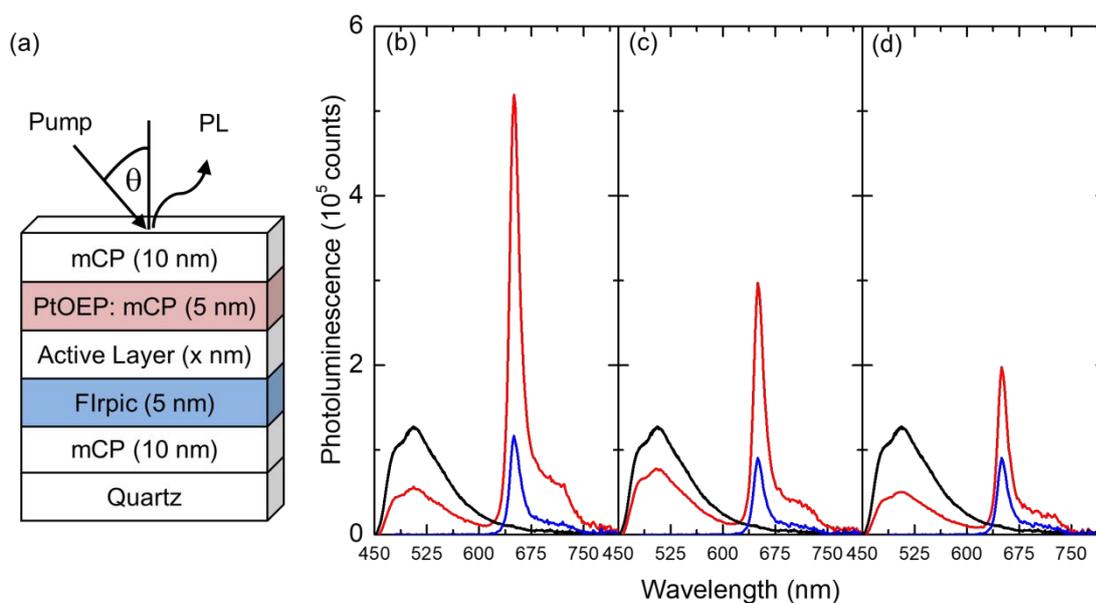
Figure 3: (a) Multilayer thin film architecture for investigating the triplet L_D for BPhen and its derivatives. The structure is pumped at a wavelength of λ=430 nm where a majority of excitons are generated in the FIrpic injection layer. The excitons that diffuse through BPhen and its derivatives are detected using 5 wt.% PtOEP doped in mCP. The photoluminescence spectra are collected for the multilayer structures FIrpic/mCP (10 nm)/mCP (black line); FIrpic/active layer (10 nm)/5 wt.% PtOEP:mCP (red line) and mCP/ active layer(10 nm)/5 wt.% PtOEP:mCP (blue line), where the active layer is (b)BPhen, (c) BPhen-Cl$_2$ or (d) BCP.
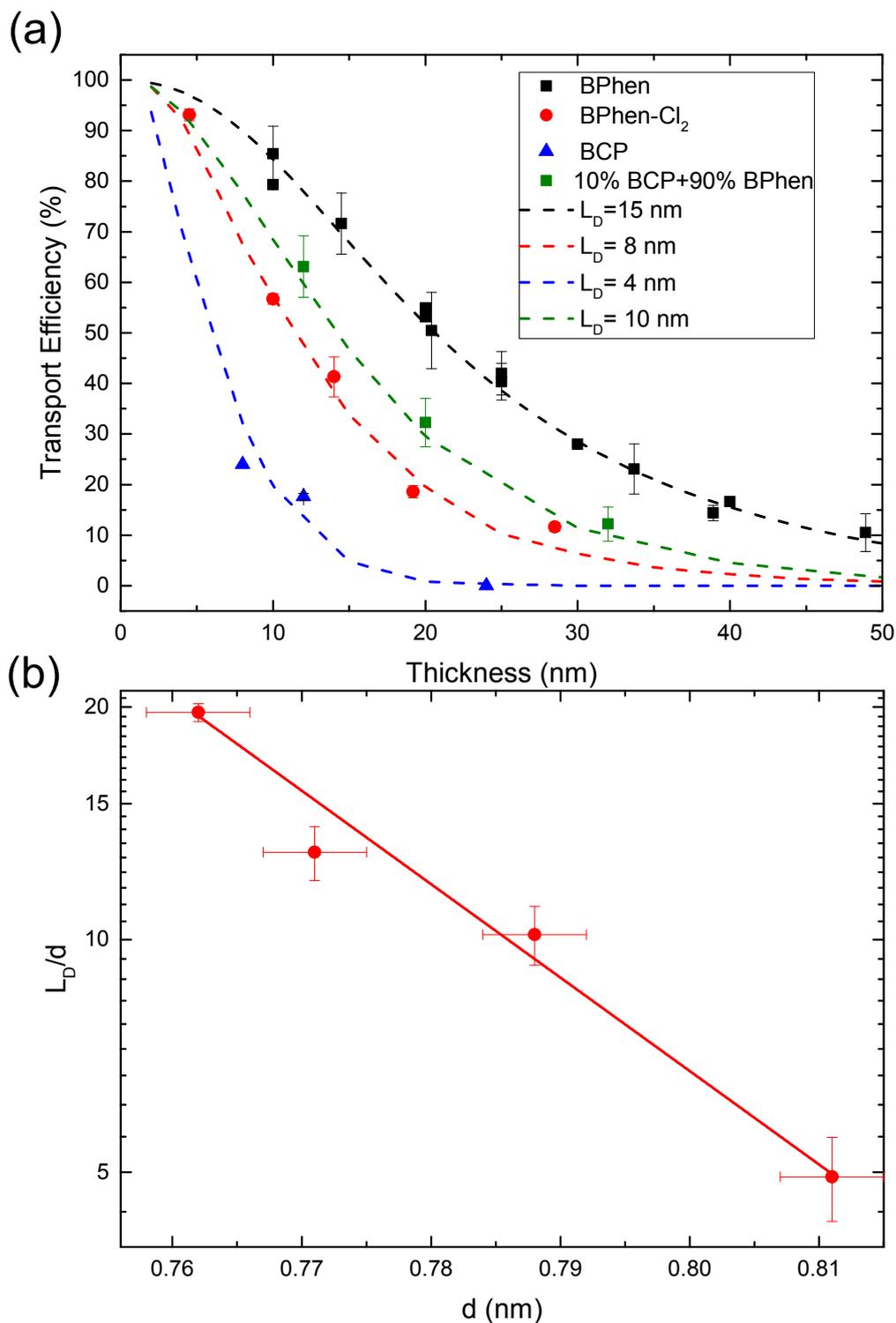
Figure 4: (a) Experimental (symbols) and simulated (lines) transport efficiency as a function of active layer thickness for different values of the triplet L_D. (b) Measured triplet L_D divided by the intermolecular spacing (d) plotted as a function of the intermolecular spacing (d) for BPhen and its derivatives. The solid line is a linear fit through the data points.

REFERENCES

1   H. Uoyama, K. Goushi, K. Shizu, H. Nomura and C. Adachi, *Nature*, 2012, **492**, 234–238.

2   F. B. Dias, K. N. Bourdakos, V. Jankus, K. C. Moss, K. T. Kamtekar, V. Bhalla, J. Santos, M. R. Bryce and A. P. Monkman, *Adv. Mater.*, 2013, **25**, 3707–3714.

3   D. Di, A. S. Romanov, L. Yang, J. M. Richter, J. P. H. Rivett, S. Jones, T. H. Thomas, M. Abdi Jalebi, R. H. Friend, M. Linnolahti, M. Bochmann and D. Credgington, *Science (80-.).*, 2017, **356**, 159–163.

4   C. Adachi, M. a. Baldo, M. E. Thompson and S. R. Forrest, *J. Appl. Phys.*, 2001, **90**, 5048–5051.

5   A. Rao, M. W. B. Wilson, J. M. Hodgkiss, S. Albert-Seifried, H. Bässler and R. H. Friend, *J. Am. Chem. Soc.*, 2010, **132**, 12698–12703.

6   S. M. Menke and R. J. Holmes, *Energy Environ. Sci.*, 2014, **7**, 499–512.

7   S. R. Yost, E. Hontz, S. Yeganeh and T. Van Voorhis, *J. Phys. Chem. C*, 2012, **116**, 17369–17377.

8   S.-B. Rim, R. F. Fink, J. C. Schöneboom, P. Erk and P. Peumans, *Appl. Phys. Lett.*, 2007, **91**, 173504.

9   R. R. Lunt, J. B. Benziger and S. R. Forrest, *Adv. Mater.*, 2010, **22**, 1233–1236.

10   H. Najafov, B. Lee, Q. Zhou, L. C. Feldman and V. Podzorov, *Nat. Mater.*, 2010, **9**, 938.

11   P. M. Beaujuge and J. M. J. Fréchet, *J. Am. Chem. Soc.*, 2011, **133**, 20009–20029.

12   T. K. Mullenbach, K. A. McGarry, W. A. Luhman, C. J. Douglas and R. J. Holmes, *Adv. Mater.*, 2013, **25**, 3689–3693.

13   O. V. Mikhnenko, J. Lin, Y. Shu, J. E. Anthony, P. W. M. Blom, T.-Q. Nguyen and M. A. Loi, *Phys. Chem. Chem. Phys.*, 2012, **14**, 14196.

14   M. Grover and R. Silbey, *J. Chem. Phys.*, 1971, **54**, 4843–4851.

15   Y. Long, G. J. Hedley, A. Ruseckas, M. Chowdhury, T. Roland, L. A. Serrano, G. Cooke

and I. D. W. Samuel, *ACS Appl. Mater. Interfaces*, 2017, **9**, 14945–14952.

16   Z. Masri, A. Ruseckas, E. V. Emelianova, L. Wang, A. K. Bansal, A. Matheson, H. T. Lemke, M. M. Nielsen, H. Nguyen, O. Coulembier, P. Dubois, D. Beljonne and I. D. W. Samuel, *Adv. Energy Mater.*, 2013, **3**, 1445–1453.

17   P. Irkhin and I. Biaggio, *Phys. Rev. Lett.*, 2011, **107**, 017402.

18   C. Wu, P. I. Djurovich and M. E. Thompson, *Adv. Funct. Mater.*, 2009, **19**, 3157–3164.

19   R. C. Powell and Z. G. Soos, *J. Lumin.*, 1975, **11**, 1–45.

20   T. Förster, *Discuss. Faraday Soc.*, 1959, **27**, 7–17.

21   J. Baumann and M. D. Fayer, *J. Chem. Phys.*, 1986, **85**, 4087–4107.

22   S. M. Menke, W. A. Luhman and R. J. Holmes, *Nat. Mater.*, 2013, **12**, 152–157.

23   S. M. Menke and R. J. Holmes, *ACS Appl. Mater. Interfaces*, 2015, **7**, 2912–2918.

24   D. L. Dexter, *J. Chem. Phys.*, 1953, **21**, 836.

25   D. B. Dement, V. E. Ferry, R. J. Holmes, T. Zhang, D. B. Dement, V. E. Ferry and R. J. Holmes, *Nat. Commun.*, 2019, **10**, 1156.

26   Y. Kawamura, H. Sasabe and C. Adachi, *Jpn. J. Appl. Phys.*, 2004, **43**, 7729–7730.

27   H. F. Xiang, Z. X. Xu, V. A. L. Roy, C. M. Che and P. T. Lai, *Rev. Sci. Instrum.*, 2007, **78**, 034104.

28   P. Peumans, A. Yakimov and S. R. Forrest, *J. Appl. Phys.*, 2003, **93**, 3693–3723.

29   R. R. Lunt, N. C. Giebink, A. a. Belak, J. B. Benziger and S. R. Forrest, *J. Appl. Phys.*, 2009, **105**, 053711.

30   D. Rai and R. J. Holmes, *Phys. Rev. Appl.*, 2019, **11**, 014048.

31   D. Rai and R. J. Holmes, *J. Mater. Chem. C*, 2019, **7**, 5695–5701.

32   R. J. Holmes, S. R. Forrest, Y.-J. Tung, R. C. Kwong, J. J. Brown, S. Garon and M. E. Thompson, *Appl. Phys. Lett.*, 2003, **82**, 2422–2424.

33   P. B. Merkel and J. P. Dinnocenzo, *J. Phys. Chem. A*, 2008, **112**, 10790–10800.

34   Z. Li, W. E. Lee and W. C. Galley, *Biophys. J.*, 1989, **56**, 361–367.

35   G. B. Strambini and W. C. Galley, *Chem. Phys. Lett.*, 1976, **39**, 257–260.

36   C. Curutchet and A. A. Voityuk, *J. Phys. Chem. C*, 2012, **116**, 22179–22185.

37   A. R. S. Kandada, G. Grancini, A. Petrozza, S. Perissinotto, D. Fazzi, S. S. K. Raavi and G. Lanzani, *Sci. Rep.*, 2013, **3**, 2073.
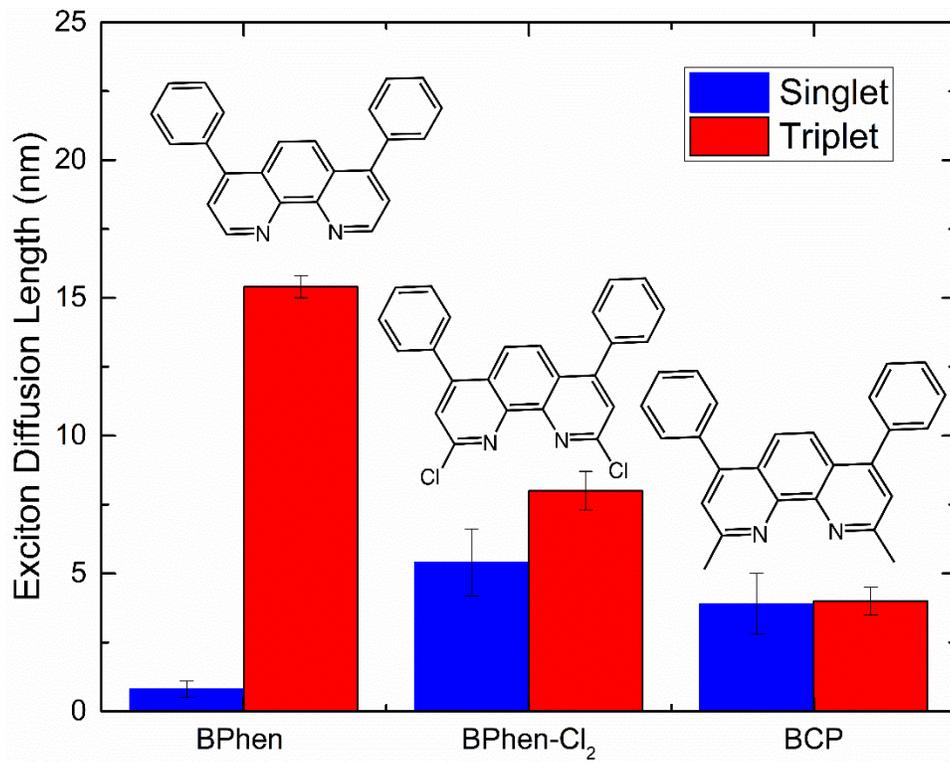
Systematic investigation of singlet and triplet exciton diffusion with changes in molecular structure and intermolecular separation for phenanthroline derivatives.